Ultrashort pulse measurements by interferometric spectrogram

Li-Fan Yang, Shih-Lun Lin, Shang-Da Yang*

Institute of Photonics Technologies, National Tsing Hua University, Hsinchu 30013, Taiwan
*shangda@ee.nthu.edu.tw

Abstract: We experimentally demonstrate that an interferometric spectrogram (i.e., fringe- and frequency-resolved autocorrelation trace) with high signal-to-noise ratio can be processed by three different procedures to accurately retrieve the spectral phase profile. We also show that the data redundancy built in the interferometric spectrogram permits simultaneous retrieval of multiple spectral phase solutions, and their weighted average may give a highly robust result against the measurement noise.

OCIS codes: (320.7100) Ultrafast measurement; (320.7110) Ultrafast nonlinear optics; (120.3180) Interferometry.

References and links

1. H. T. Shang, "Chromatic dispersion measurement by white-light interferometry on metre-length single-mode optical fibres," Electron. Lett. **17**(17), 603–605 (1981).
2. N. Dudovich, D. Oron, and Y. Silberberg, "Single-pulse coherently controlled nonlinear Raman spectroscopy and microscopy," Nature **418**(6897), 512–514 (2002).
3. E. Matsubara, K. Yamane, T. Sekikawa, and M. Yamashita, "Generation of 2.6 fs optical pulses using induced-phase modulation in a gas-filled hollow fiber," J. Opt. Soc. Am. B **24**(4), 985–989 (2007).
4. Z. Jiang, C.-B. Huang, D. E. Leaird, and A. M. Weiner, "Optical arbitrary waveform processing of more than 100 spectral comb lines," Nat. Photonics **1**(8), 463–467 (2007).
5. D. N. Fittinghoff, J. L. Bowie, J. N. Sweetser, R. T. Jennings, M. A. Krumbüugel, K. W. Delong, R. Trebino, and I. A. Walmsley, "Measurement of the intensity and phase of ultraweak, ultrashort laser pulses," Opt. Lett. **21**(12), 884–886 (1996).
6. I. Kang, and C. Dorrer, "Method of optical pulse characterization using sinusoidal optical phase modulations," Opt. Lett. **32**(17), 2538–2540 (2007).
7. R. Trebino, P. Bowlan, P. Gabolde, X. Gu, S. Akturk, and M. Kimmel, "Simple devices for measuring complex ultrashort pulses," Laser Photon. Rev. **3**(3), 314–342 (2009).
8. C. Iaconis, and I. A. Walmsley, "Spectral phase interferometry for direct electric-field reconstruction of ultrashort optical pulses," Opt. Lett. **23**(10), 792–794 (1998).
9. H. Miao, D. E. Leaird, C. Langrock, M. M. Fejer, and A. M. Weiner, "Optical arbitrary waveform characterization via dual-quadrature spectral shearing interferometry," Opt. Express **17**(5), 3381–3389 (2009).
10. D. N. Fittinghoff, K. W. DeLong, R. Trebino, and C. L. Ladera, "Noise sensitivity in frequency-resolved optical-gating measurements of ultrashort pulses," J. Opt. Soc. Am. B **12**(10), 1955–1967 (1995).
11. S.-D. Yang, A. M. Weiner, K. R. Parameswaran, and M. M. Fejer, "Ultrasensitive second-harmonic generation frequency-resolved optical gating by aperiodically poled LiNbO3 waveguides at 1.5 microm," Opt. Lett. **30**(16), 2164–2166 (2005).
12. I. Amat-Roldán, I. Cormack, P. Loza-Alvarez, E. Gualda, and D. Artigas, "Ultrashort pulse characterisation with SHG collinear-FROG," Opt. Express **12**(6), 1169–1178 (2004).
13. G. Stibenz, and G. Steinmeyer, "Interferometric frequency-resolved optical gating," Opt. Express **13**(7), 2617–2626 (2005).
14. I. Amat-Roldán, I. G. Cormack, P. Loza-Alvarez, and D. Artigas, "Measurement of electric field by interferometric spectral trace observation," Opt. Lett. **30**(9), 1063–1065 (2005).
15. I. Amat-Roldan, D. Artigas, I. G. Cormack, and P. Loza-Alvarez, "Simultaneous analytical characterisation of two ultrashort laser pulses using spectrally resolved interferometric correlations," Opt. Express **14**(10), 4538–4551 (2006).
16. S.-D. Yang, C.-S. Hsu, S.-L. Lin, H. Miao, C.-B. Huang, and A. M. Weiner, "Direct spectral phase retrieval of ultrashort pulses by double modified one-dimensional autocorrelation traces," Opt. Express **16**(25), 20617–20625 (2008).
17. S.-D. Yang, C.-S. Hsu, S.-L. Lin, Y.-S. Lin, C. Langrock, and M. M. Fejer, "Ultrasensitive direct-field retrieval of femtosecond pulses by modified interferometric field autocorrelation," Opt. Lett. **34**(20), 3065–3067 (2009).
18. C.-S. Hsu, and S.-D. Yang, "Robustness enhancement of iteration-free spectral phase retrieval by interferometric second-harmonic trace," presented at the Conference on Lasers & Electro Optics, Baltimore, Maryland, USA, 6–11 May, 2007.

1. Introduction

Measuring the spectral phase profiles of broadband optical signals is essential in a variety of applications, such as dispersion characterization of optical media [1], coherently controlled nonlinear spectroscopy [2], quasi-one-optical-cycle pulse compression [3], and high repetition rate pulse trains from externally-modulated optical frequency combs [4]. Linear measurement techniques have high sensitivity but normally require a synchronized and precisely characterized reference [5] or a high-speed (tens of gigahertz) modulator [6], which could be unavailable in the intermediate stage of a long-haul telecommunication link or at wavelengths other than the telecommunications band. In terms of self-referenced nonlinear measurement techniques, time-frequency and interferometric techniques are most widely used, which employ spectrally resolved autocorrelation trace (i.e., spectrogram) [7] and spectrally sheared interferogram [8, 9], respectively. Time-frequency techniques, such as frequency-resolved optical gating (FROG) [7], can retrieve the complex field with excellent robustness [10] and extremely high sensitivity [11]. However, they are subject to slower refresh rate due to the inherent data redundancy and the requirement of iterative data inversion (to solve the two-dimensional phase retrieval problem). Interferometric spectral shearing techniques can rapidly deliver the spectral phase profile without iteration, but require demanding spectral resolution [8] or two highly coherent continuous-wave (CW) tones [9]. It becomes promising to combine the advantages of time-frequency and interferometric techniques by measuring the fringe- and frequency-resolved autocorrelation trace (i.e., interferometric spectrogram), which can be acquired by a collinear Michelson interferometer (MI) and a thin second-harmonic generation (SHG) crystal. An early work using the interferometric spectrogram for ultrashort pulse measurement was reported in Reference [12], where the standard SHG FROG trace (i.e., the non-interferometric components of the data) was extracted for iterative data inversion. This method permits simpler experimental configuration and enhanced error-checking capability, but inherits all the restrictions of time-frequency techniques. Two novel methods, fundamental-modulation (FM) FROG [13], and measurement of electric field by interferometric spectral trace observation (MEFISTO) [14, 15], were demonstrated to iteratively reconstruct the complex field and analytically retrieve the spectral phase by processing the interferometric components of the interferometric spectrogram, respectively. These methods are free from the requirements of excess spectral resolution and CW tones, however, the enormous data redundancy built in the interferometric spectrogram (more than that of the standard FROG trace) makes these pulse measurement techniques less efficient. We have recently demonstrated a new technique to analytically retrieve the spectral phase and amplitude profiles using two one-dimensional modified interferometric field autocorrelation (MIFA) traces acquired by a collinear MI and a thick SHG crystal controlled at two different temperatures [16, 17]. The MIFA method enables unprecedented measurement sensitivity [17], and greatly reduces the system complexity and data redundancy. In this literature, we demonstrate that the two MIFA traces used for complex field retrieval can also be obtained by sampling the interferometric spectrogram at two optical frequencies. This linear spectral sampling approach can result in more accurate MIFA traces, which are free from the error induced by the *sinc*-shaped phase-matching spectrum. It also relaxes the criterion of crystal thickness, permitting measurement of pulses of a wide range of durations by using a single nonlinear crystal. We also show that the enormous data redundancy built in the interferometric spectrogram could be practically useful. First, the consistency among the spectral phase profiles retrieved by FROG, MEFISTO and MIFA methods using the same interferometric spectrogram provides a solid evidence about the measurement fidelity. Second, sampling the interferometric spectrogram at different optical frequencies (for MIFA) or delay-frequencies (for MEFISTO) [18] gives rise to different solutions of the spectral phase profile. Compared with the single solution derived in the standard MIFA or MEFISTO method, the weighted average of the multiple solutions is more robust against measurement noise in the presence of a data set with low signal-to-noise ratio (SNR). Our experiments show that averaging the 45 phase curves retrieved by the multiple-sampling MIFA method

can reduce the root-mean-square (rms) error of the reconstructed temporal intensity by a factor of 2.7 when the SNR of the measured interferometric spectrogram is as low as 7.9.

2. Theory

Assuming the unknown pulse has a complex temporal envelope $E(t)$ and a carrier frequency f_0. The pulse is sent into a collinear MI to produce a pulse pair with variable delay τ, then passes through a thin nonlinear crystal with sufficiently broad phase-matching bandwidth for SHG. The interferometric spectrogram is acquired by measuring the second-harmonic power spectrum as a function of delay τ [12]:

$$
\begin{aligned}
I^{SHG}(f,\tau) \propto{}& I_{SHG}(f) + 2I_{FROG}^{SHG}(f,\tau) + I_{SHG}(f)\cos\left[2\pi(2f_0+f)\tau\right] \\
&+ 2\mathrm{Re}\left\{E_{SHG}^{*}(f)E_{FROG}^{SHG}(\tau,f)\left[\exp(-j2\pi f_0\tau)+\exp\left(j2\pi(f_0+f)\tau\right)\right]\right\}
\end{aligned}
\tag{1}
$$

where $E_{SHG}(f) \propto F_t\{E^2(t)\}$, $E_{FROG}^{SHG}(f,\tau) \propto F_t\{E(t)E(t-\tau)\}$, $F_t\{\ \}$ means the Fourier transform with respect to the time variable t, $I_{SHG}(f) \propto \left|E_{SHG}(f)\right|^2$, and $I_{FROG}^{SHG}(f,\tau) \propto \left|E_{FROG}^{SHG}(f,\tau)\right|^2$. Fig. 1a illustrates the simulated interferometric spectrogram $I^{SHG}(f,\tau)$ due to a transform-limited Gaussian pulse with $E(t) = \exp\left[-2\ln 2(t/\Delta t)^2\right]$ and $f_0 = 5/\Delta t$, where Δt represents the full-width at half maximum (FHWM) of $\left|E(t)\right|^2$. The first and second terms of the right hand side of Eq. (1) represent the τ-independent signal background (second-harmonic power spectrum of the pulse) and the standard SHG FROG trace, respectively. The remaining interferometric terms result in dense fringes along the τ-axis for all optical frequency components and fringes along the f-axis for larger delay values.
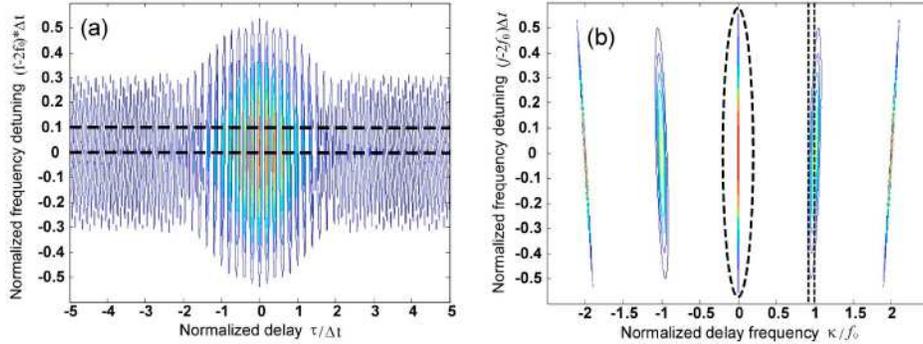

Fig. 1. (a) Simulated interferometric spectrogram of a transform-limited Gaussian pulse defined in the main text, and (b) its Fourier transform with respect to delay. (For clarity, Fig. 1b is manipulated to highlight the components around $\kappa = \pm f_0$)

Different terms of Eq. (1) can be separated by taking one-dimensional Fourier transform for $I^{SHG}(f,\tau)$ with respect to the delay variable τ, i.e., $Y^{SHG}(f,\kappa) = F_\tau\{I^{SHG}(f,\tau)\}$, where κ denotes the delay-frequency variable (Fig. 1b). The standard SHG FROG trace $I_{FROG}^{SHG}(f,\tau)$ can be obtained by extracting the low-delay-frequency components of $Y^{SHG}(f,\kappa)$ (Fig. 1b, enclosed by the dashed ellipse) and eliminating the signal background, from which an iterative algorithm can be used to reconstruct the complex field of the unknown pulse. The last term of Eq. (1) is mapped to the components of $Y^{SHG}(f,\kappa)$ centered at $\kappa = \pm f_0$, which

could be used in retrieving the pulse information analytically. In the MEFISTO method [14], a spectral phase difference function is obtained by sampling $Y^{SHG}(f,\kappa)$ at two slightly separated delay-frequencies $\kappa_1 = f_0$ and $\kappa_2 = f_0 - \delta$ (Fig. 1b, dashed lines), from which the spectral phase can be analytically determined (to a resolution of δ) by direct integration. In the previous demonstrations of the MIFA method [16,17], we acquired two one-dimensional interferometric traces using a collinear MI and thick nonlinear crystals with narrow phase-matching bandwidth and slightly detuned central phase-matching frequencies $f_1 = 2f_0$ and $f_2 = 2(f_0 + \Delta)$. Analysis of the two MIFA traces gives a spectral phase difference function and a spectral amplitude rational function that can be used to analytically recover the complex field (to a resolution of 2Δ). Since the phase-matching spectrum of a uniform nonlinear crystal is a *sinc*-function with side lobes, the MIFA traces resulting from this nonlinear spectral sampling approach may have some small amount of error. In the absence of a thick nonlinear crystal, the required MIFA traces can also be obtained by directly sampling the interferometric spectrogram $I^{SHG}(f,\tau)$ at two different optical frequencies with a small detuning 2Δ (Fig. 1a, dashed lines). The corresponding linear spectral sampling function (provided by the angular dispersion optics) can be closer to an ideal δ-function, leading to more accurate MIFA traces. This alternative approach also relaxes the criterion of crystal thickness. As a result, a single nonlinear crystal can be used to characterize pulses of very different durations by MIFA. Although both MIFA and MEFISTO utilize the interferometric components of the interferometric spectrogram, they are essentially different in terms of: (1) MIFA can retrieve the spectral phase and amplitude [17], while MEFISTO only gives the spectral phase. (2) MIFA analyzes $I^{SHG}(f_{1,2},\tau)$ (or equivalently $Y^{SHG}_{\kappa \approx 0}(f_{1,2},\kappa)$, $Y^{SHG}_{\kappa \approx f_0}(f_{1,2},\kappa)$) [16], while MEFISTO uses $Y^{SHG}_{\kappa \approx f_0}(f,\kappa_{1,2})$. The latter difference means that there is no need to compute $Y^{SHG}(f,\kappa)$ to obtain the two MIFA traces (in contrast to MEFISTO), which is time-consuming when measuring pulses whose temporal envelope covers a large number of carrier fringes.

The advantages of measuring interferometric spectrogram in pulse retrieval are twofold. First, it can provide solid evidence for the measurement fidelity if the single interferometric spectrogram results in mutually consistent solutions obtained by the three different methods (FROG, MEFISTO, and MIFA). Second, the built-in data redundancy of the interferometric spectrogram permits simultaneous retrieval of multiple spectral phase solutions by sampling more traces from different parts of $I^{SHG}(f,\tau)$ (MIFA) or $Y^{SHG}(f,\kappa)$ (MEFISTO). The weighted average of these solutions is expected to be more robust against the measurement noise. In practice, determining the spectral phase difference function of the MEFISTO method needs to evaluate two rational functions [15]:

$$\Omega(f,\kappa_i) = \frac{Y^{SHG}(f,\kappa_i)}{4\chi_{eff} U_{SHG}(f) U(f + f_0 - \kappa_i) U(\kappa - f_0)}, (i = 1, 2), \qquad (2)$$

where $U(f)$, $U_{SHG}(f)$ are the normalized fundamental and second-harmonic spectral magnitudes with unit peak value, and χ_{eff} equals the peak value of the product of the spectral magnitudes $|E^2(f)E_{SHG}(f)|$ ($E(f) = F_t\{E(t)\}$) [15]. All the parameters $U(f)$, $U_{SHG}(f)$, and χ_{eff} can be derived from the interferometric spectrogram itself. However, Eq. (2) is vulnerable to the noise contamination especially at the weak spectral wings for it involves with the "ratio" of two spectral functions. This feature increases the required SNR for reliable MEFISTO measurements and hampers the employment of multiple-sampling MEFISTO scheme.

3. Experiments

Figure 2a shows the experimental setup of interferometric spectrogram measurement. The signal pulse comes from a passively mode-locked Er-doped fiber laser with 50 MHz repetition rate, 1560 nm central wavelength (f_0 ~ 192.18 THz), 12 nm bandwidth (FWHM of the power spectrum), and 1 mW average power. A section of dispersion compensating fiber (DCF) is inserted to partially compensate for the accumulated dispersion of the fiber link. The signal pulse is combined with a 1480 nm CW reference by a wavelength division multiplexer (WDM) and launched into a free-space collinear MI via a collimator. The interfered waves from one of the two output arms of the MI return to the fiber link, and are separated from the input waves by a circulator. A second WDM was used to spectrally separate the interfered reference and signal waves, and the corresponding delay-dependent average powers, $I_{CW}(\tau)$ and $I_{pulse}(\tau)$, are measured by two InGaAs photodetectors, respectively. The optical beam from the other output arm of the MI is focused to a 1-mm-thick BBO crystal for broadband SHG, and recorded by a spectrometer and an un-cooled CCD array (Jobin Yvon, Sygnature) with 50 ms integration time. The delay τ of the interferometric spectrogram $I^{SHG}(f,\tau)$ is scanned over a range of 5 ps and has a step size of 1.3 fs, roughly equal to the Nyquist criterion of $0.25 f_0$. Since the MEFISTO and MIFA methods require a data set of interferometric precision, we use the trace $I_{CW}(\tau)$ to correct the fluctuated delay step size due to the unstable delay scanning. Figure 2b shows that the fringe-corrected field autocorrelation trace $I_{pulse}(\tau)$ can produce a fundamental power spectrum (dashed) in good agreement with that directly measured by an optical spectrum analyzer (solid). The small spectral bump near 194.3 THz can still be resolved, proving the usefulness of our fringe correction process.
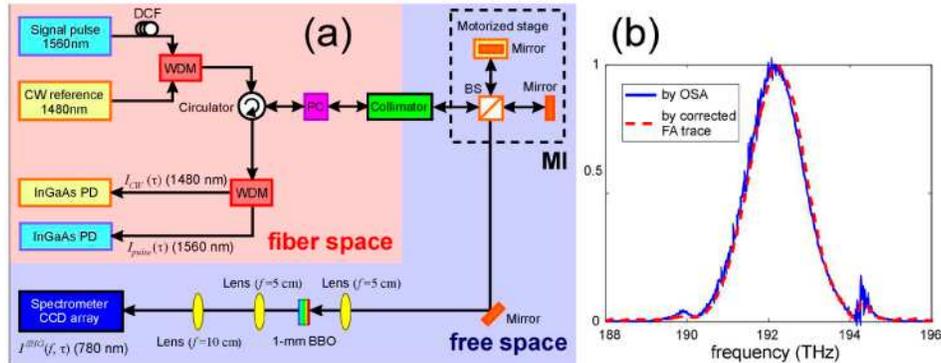

Fig. 2. (a) Experimental setup of interferometric spectrogram measurement. DCF: dispersion compensating fiber. WDM: wavelength division multiplexer. PC: polarization controller. BS: beam splitter. MI: Michelson interferometer. PD: Photodetector. (b) Fundamental power spectra of the signal pulse measured by an optical spectrum analyzer (OSA) (solid), and fringe-corrected field autocorrelation (FA) trace (dashed), respectively.

Figure 3a shows the experimentally measured fringe-corrected interferometric spectrogram $I^{SHG}(f,\tau)$ of the signal pulse, where the delay-independent signal background, the dense fringes along the delay axis, and the additional fringes along the optical frequency axis at large delay values are evident. The corresponding SNR value (defined as the ratio of the peak value to the average noise level of the measured interferometric spectrogram) is 39. The Fourier transform of $I^{SHG}(f,\tau)$ (Fig. 3b) exhibits five components centered at delay-frequencies of $\kappa = 0$, $\pm f_0$, $\pm 2f_0$, respectively. The standard SHG FROG trace $I_{FROG}^{SHG}(f,\tau)$ is extracted from $Y_{\kappa \approx 0}^{SHG}(f,\kappa)$. Iterative data inversion using commercial software (Femtosoft,

FROG3) gives rise to a similar trace with a low FROG error of 2.65×10^{-3} and a spectral phase curve $\psi_{FROG}(f)$ (Fig. 3c, dotted). Another two spectral phase profiles $\psi_{MIFA}(f)$ (Fig. 3c, dashed) and $\psi_{MEFISTO}(f)$ (Fig. 3c, dash-dot) are retrieved by processing the data traces, $I^{SHG}(2f_0, \tau)$, $I^{SHG}(2(f_0 + \Delta), \tau)$ (with $\Delta = 60$ GHz) and $Y^{SHG}(f, f_0)$, $Y^{SHG}(f, f_0 - \delta)$ (with $\delta = 200$ GHz), respectively. The three phase curves are in good agreement with one another over the frequency range where the spectral power remains noticeable. The temporal intensity profiles (Fig. 3d) derived by the power spectrum measured by OSA (Fig. 3c, solid) and the corresponding spectral phase profiles are fairly consistent, proving the reliability of the proposed approach.
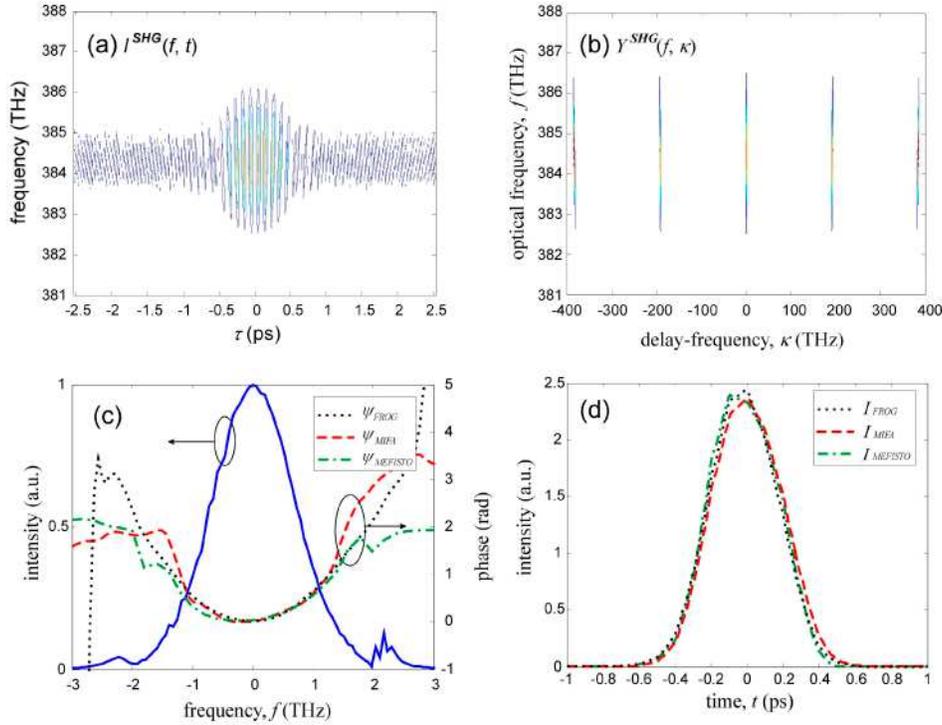

Fig. 3. (a) Experimentally measured interferometric spectrogram, and (b) its Fourier transform with respect to delay. For clarity, Fig. 3b is manipulated to highlight the components around $\kappa = \pm f_0$. (c) Spectral phase profiles, and (d) temporal intensity profiles measured by FROG (dotted), MIFA (dashed), and MEFISTO (dash-dot), respectively. The solid line in Fig. 3c represents the fundamental power spectrum measured by OSA.

To further verify our scheme, we insert a 1.9-m-long single mode fiber (SMF) into the link and then measure the broadened pulse by the same procedures. Figure 4a shows the experimentally measured fringe-corrected interferometric spectrogram $I^{SHG}(f, \tau)$ of the broadened signal pulse, which extends a wider delay range compared to that in Fig. 3a. Figure 4b shows the spectral phase curves retrieved by the three different methods. $\psi_{FROG}(f)$ (dotted) and $\psi_{MIFA}(f)$ (dashed) remain in good agreement, while $\psi_{MEFISTO}(f)$ (dash-dot) has significant distortion. This is partially attributed to the fact that the determination of the spectral phase function by the MEFISTO method is more sensitive to noise contamination, while a broader pulse has weaker SHG yield and reduces the SNR of the data trace (28, compared to 39 of Fig. 3a). The difference between the spectral phase curves [$\psi_{FROG}(f)$ or $\psi_{MIFA}(f)$] measured before (Fig. 3c) and after (Fig. 4b) the insertion of the 1.9-m-long SMF

can be used to characterize the dispersion of the fiber. Fitting the difference curve gives rise to a dispersion value of $D = 17.9$ ps/nm/km, slightly deviated from the specifications by ~5%. The discrepancy may arise from the fluctuation of the pulse source during the long (~30 minutes) data acquisition, and the noise-induced error that is exacerbated in the presence of the small amount of dispersion of the short (1.9-m-long) SMF.
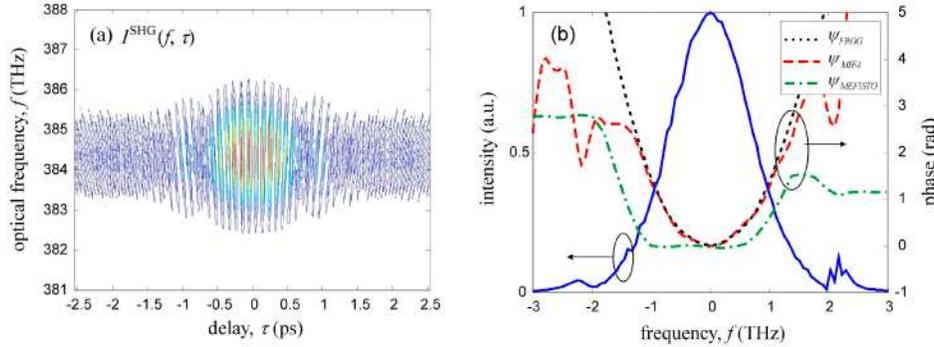

Fig. 4. (a) Experimentally measured interferometric spectrogram of the signal pulse broadened by a 1.9-m-long SMF. (b) Spectral phase profiles measured by FROG (dotted), MIFA (dashed), and MEFISTO (dash-dot), respectively. The solid line represents the fundamental power spectrum measured by OSA.

Figure 5 shows the usefulness of sampling multiple pairs of MIFA traces from the interferometric spectrogram for pulse characterizations. We tune the polarization controller to attenuate the SHG yield, lowering the SNR of the measured interferometric spectrogram of the broadened signal pulse to 7.9. The spectral phase profile $\psi_{MIFA}^{(1)}(f)$ retrieved by the standard MIFA method (Fig. 5a, dash-dot) using one pair of MIFA traces sampled from $I^{SHG}(f,\tau)$ is appreciably deviated from the reference curve measured by FROG at higher SNR value (Fig. 5a, dotted, i.e., the dotted curve in Fig. 4b). Additional spectral phase solutions $\psi_{MIFA,i}^{(1)}(f)$ can be derived by sampling $I^{SHG}(f,\tau)$ at different optical frequencies $f = 2f_i$ and $f = 2(f_i + \Delta)$, as long as $|f_i - f_0|$ is smaller than the bandwidth of the signal pulse. The weighted average of N spectral phase solutions (Fig. 5a, dash), i.e.,

$$\psi_{MIFA}^{(N)}(f) = \sum_{i=1}^{N} \psi_{MIFA,i}^{(1)}(f) \cdot I(f_i), \tag{3}$$

could be closer to the reference profile, where $I(f)$ denotes the fundamental power spectrum measured by OSA (Fig. 5a, solid). However, increasing the number of sampled MIFA traces does not necessarily improve the measurement result, for $I^{SHG}(2f_i,\tau)$ and $I^{SHG}(2(f_i + \Delta),\tau)$ may have lower SNR and produce worse $\psi_{MIFA,i}^{(1)}(f)$ if f_i is far away from the carrier frequency f_0. We use the rms error of the temporal intensity, i.e.,

$$\varepsilon = \sqrt{\int \left[I_{MIFA}(t) - I_{FROG}(t) \right]^2 dt} \Big/ \left[\int I_{FROG}(t) dt \right], \tag{4}$$

to quantitatively measure the accuracy of the MIFA measurement result, where $I_{FROG}(t)$ and $I_{MIFA}(t)$ are the temporal intensity profiles measured by FROG and MIFA, respectively. Figure 5b shows the rms error versus the number of pairs of MIFA traces N used for retrieving the spectral phase profile by Eq. (3) in this specific experiment. The error initially decreases with N due to the noise-suppression effect of the weighted average, then starts to increase again because of the inclusion of traces with lower SNR. In this specific case (the interferometric spectrogram has an SNR of 7.9), using 45 pairs of MIFA traces (covering a

spectral range of 0.72 THz, or 47% of the FWHM of the fundamental power spectrum) gives a spectral phase profile $\psi_{MIFA}^{(45)}(f)$ (Fig. 5a, dashed) with the lowest rms error of 0.074, about 2.7 times smaller than that derived by the standard MIFA method. However, the noise suppression effect and the optimal number of used MIFA trace pairs depend on the SNR of the measured interferometric spectrogram. For example, the error reduction factor and the optimal number of used MIFA trace pairs are reduced to 1.25 and 8 when the data trace has an SNR of 39. This is because that most of the solutions obtained by processing a high-quality data trace with the multiple-sampling MIFA method are fairly accurate, and the average of these solutions remains similar with the individual ones. Our experimental data show that the multi-sampling MIFA method remains useful for data traces with an SNR less than 25.
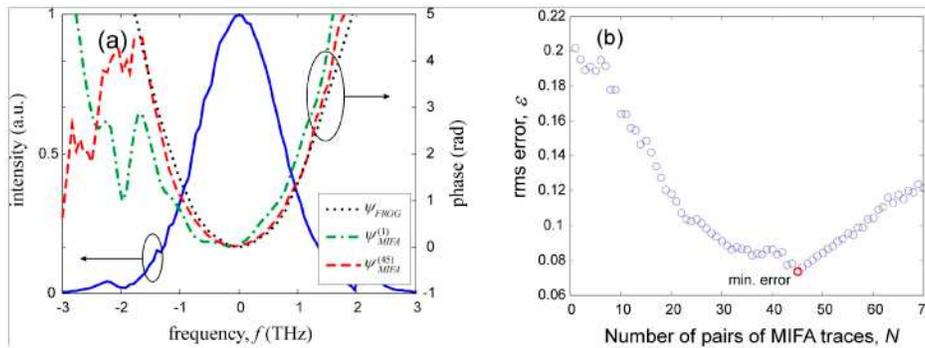

Fig. 5. (a) Spectral phase profiles measured by MIFA using 1 (dash-dot), and 45 (solid) pairs of MIFA traces sampled from the interferometric spectrogram, respectively. The spectral phase measured by FROG at SNR = 28 (dotted) is shown as a reference. (b) rms error value versus the number of pairs of MIFA traces used for retrieving the spectral profile by Eq. (3).

4. Conclusions and acknowledgments

We have experimentally demonstrated that the same interferometric spectrogram with a high SNR (e.g. 39) can be processed by three different procedures (FROG, MIFA, and MEFISTO) to accurately retrieve the spectral phase profile. The two MIFA traces used for spectral phase retrieval in our experiments are obtained by sampling the interferometric spectrogram at two optical frequencies. This linear spectral sampling approach may result in more accurate MIFA traces (than those acquired by using thick nonlinear crystal), and permit measuring pulses of a wide range of durations by using a single crystal. As the SNR of the interferometric spectrogram decreases, FROG appears most robust while MIFA and MEFISTO suffer from larger error. MEFISTO appears most sensitive to the noise contamination for it involves with the evaluation of spectral rational functions, which may have large error at the spectral wings. We also show that the data redundancy of the interferometric spectrogram could be utilized to suppress the noise-induced measurement error. Our experiments demonstrate that the multiple-sampling MIFA method can deliver a spectral phase profile similar to that obtained by FROG, even the interferometric spectrogram is quite noisy (SNR = 7.9). However, the noise suppression effect of the multiple-sampling MIFA method decreases with the increase of the SNR of the data trace. We found that the multi-sampling MIFA method remains useful for data traces with an SNR less than 25.